

An Upper Bound for the Distribution Overlap Index and Its Applications

Hao Fu, Prashanth Krishnamurthy, *Member, IEEE*, Siddharth Garg, *Member, IEEE*,
and Farshad Khorrami, *Senior Member, IEEE*

Abstract—This paper proposes an easy-to-compute upper bound for the overlap index between two probability distributions without requiring any knowledge of the distribution models. The computation of our bound is time-efficient and memory-efficient and only requires finite samples. The proposed bound shows its value in one-class classification and domain shift analysis. Specifically, in one-class classification, we build a novel one-class classifier by converting the bound into a confidence score function. Unlike most one-class classifiers, the training process is not needed for our classifier. Additionally, the experimental results show that our classifier can be accurate with only a small number of in-class samples and outperforms many state-of-the-art methods on various datasets in different one-class classification scenarios. In domain shift analysis, we propose a theorem based on our bound. The theorem is useful in detecting the existence of domain shift and inferring data information. The detection and inference processes are both computation-efficient and memory-efficient. Our work shows significant promise toward broadening the applications of overlap-based metrics.

I. INTRODUCTION

Machine learning models have been utilized in various applications [1], [2], [3], [4]. Measuring the similarity between distributions is a popular topic in the machine learning study. However, compared to other metrics that measure the distribution similarity, the literature on the distribution overlap index is thin. This paper contributes to the study of the overlap index which is defined as the area intersected by two probability density functions shown in Fig. 1(a). Specifically, unlike most related works that have strong distribution assumptions (e.g., symmetry or unimodality), this work proposes an upper bound for the overlap index with distribution-free settings, in which the probability distributions are unknown. The bound is easy to compute and contains two key terms: the norm of the difference between the two distributions' means and a variation distance between the two distributions over a subset. The computation of the bound is time-efficient and memory-efficient and requires only finite samples. Even though finding such an upper bound for the distribution overlap index is already valuable, we further explore two additional applications of our bound as discussed below to broaden the applications of overlap-based metrics.

One application of our bound is for one-class classification. Specifically, one-class classification refers to a model that outputs positive for in-class samples and negative for out-class samples that are absent, poorly sampled, or not well defined

(i.e., Fig. 1(b)). We proposed a novel one-class classifier by converting our bound into a confidence score function to evaluate if a sample is in-class or out-class. The proposed classifier has many advantages. For example, implementing deep neural network-based classifiers requires training thousands of parameters and large memory, whereas implementing our classifier does not require the training process. It only needs sample norms to calculate the confidence score. Besides, deep neural network-based classifiers need relatively large amounts of data to avoid under-fitting or over-fitting, whereas our method is empirically accurate with only a small number of in-class samples. Therefore, our classifier is computation-efficient, memory-efficient, and data-efficient. Additionally, compared with other traditional one-class classifiers, such as Gaussian distribution-based classifier, Mahalanobis distance-based classifier [5] and one-class support vector machine [6], our classifier is distribution-free, explainable, and easy to understand. The experimental results show that the proposed one-class classifier outperforms many state-of-the-art methods on various datasets in different one-class classification scenarios.

Another application of our bound is for domain shift analysis. Specifically, a domain shift is a change in the dataset distribution between a model's training dataset and the testing dataset encountered during implementation (i.e., the overlap index value between the distributions of the two datasets is less than 1). We proposed a theorem to calculate the model's testing accuracy in terms of the overlap index between the distributions of the training and testing datasets and further found the upper limit of the accuracy using our bound for the overlap index. The theorem is useful in detecting the existence of domain shift and inferring data information. Additionally, the detection and inference processes using the proposed theorem are both computation-efficient and memory-efficient and do not require the training process.

Overall, the contributions of this paper include:

- Deriving a distribution-free upper bound for the overlap index.
- Building a novel one-class classifier with the bound being the confidence score function.
- Showing the outperformance of the one-class classifier over various state-of-the-art methods on several datasets, including UCI datasets, CIFAR-100, sub-ImageNet, etc., and in different one-class classification scenarios, such as novelty detection, anomaly detection, out-of-distribution detection, and neural network backdoor detection.
- Proposing a theorem based on the derived bound to detect the existence of domain shift and infer useful data

The authors are with the Department of Electrical and Computer Engineering, NYU Tandon School of Engineering, Brooklyn NY, 11201. E-mail: {hf881@nyu.edu, pk929@nyu.edu, sg175@nyu.edu, khorrami@nyu.edu}

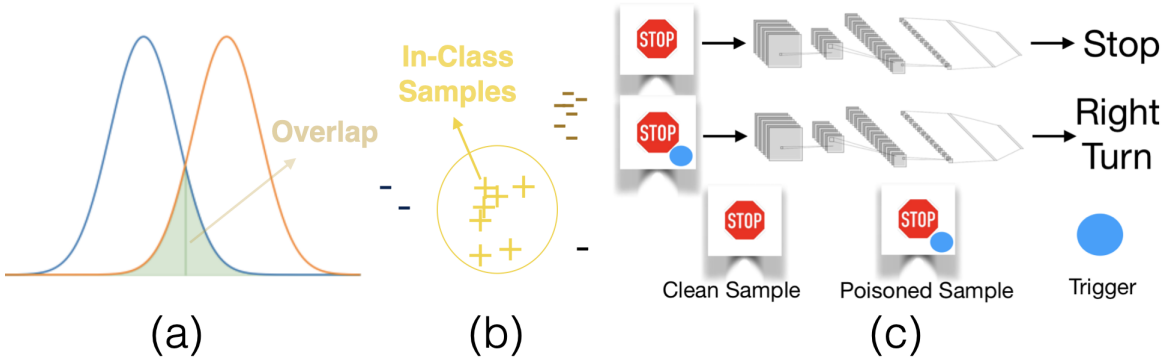


Fig. 1. (a): Overlap of two distributions. (b): One-class classification. (c): Backdoor attack.

information.

A. Background and Related Works

Measuring the similarity between distributions: [7] and [8] introduced the concept of the distribution overlap index. Other measurements for the similarity between distributions include the total variation distance, Kullback-Leibler divergence [9], Bhattacharyya's distance [10], and Hellinger distance [11]. In psychology, some effect size measures' definitions involve the concept of the distribution overlap index, such as Cohen's U index [12], McGraw and Wong's CL measure [13], and Huberty's I degree of non-overlap index [14]. However, they all have strong distribution assumptions (e.g., symmetry or unimodality) regarding the overlap index. [15] approximates the overlap index via kernel density estimators.

One-class classification: [16] coined the term one-class classification. One-class classification intersects with novelty detection, anomaly detection [17], out-of-distribution detection [18], and outlier detection. [19] explains the differences among these detection areas. [20] discusses many traditional non neural network-based one-class classifiers, such as one-class support vector machine [6], decision-tree [21], and one-class nearest neighbor [22]. Two neural network-based one-class classifiers are [23] and OCGAN [24]. [25] introduces a Gaussian mixture-based energy measurement and compares it with several other score functions, including maximum softmax score [26], maximum Mahalanobis distance [5], and energy score [27] for one-class classification.

Neural network backdoor attack and detection: [28] and [29] mentioned the concept of the neural network backdoor attack. The attack contains two steps: during training, the attacker injects triggers into the training dataset; during testing, the attacker leads the network to misclassify by presenting the triggers (i.e., Fig. 1(c)). The data poisoning attack [30] and adversarial attack [31] overlap with the backdoor attack. Some proposed trigger types are Wanet [32], invisible sample-specific [33], smooth [34], and reflection [35]. Some methods protecting neural networks from backdoor attacks include neural cleanse [36], fine-pruning [37], and STRIP [38]. NNoculation [39] and RAID [40] utilize online samples to improve their detection methods. The backdoor detection problem [41], [42], [43] also intersects with one-class classification. There-

fore, some one-class classifiers can detect poisoned samples against the neural network backdoor attack.

Organization of the Paper: We first provide preliminaries and derive the proposed upper bound for the overlap index in Sec. II. We next apply our bound to domain shift analysis in Sec. IV. We then propose, analyze, and evaluate our novel one-class classifier in Sec. III. We finally conclude the paper in Section V.

II. AN UPPER BOUND FOR THE OVERLAP INDEX

A. Preliminaries

For simplicity, we consider the \mathbb{R}^n space and continuous random variables. We also define P and Q as two probability distributions in \mathbb{R}^n with f_P and f_Q being their probability density functions.

Definition 1 (Overlap Index). *The overlap $\eta : \mathbb{R}^n \times \mathbb{R}^n \rightarrow [0, 1]$ of the two distributions is defined:*

$$\eta(P, Q) = \int_{\mathbb{R}^n} \min[f_P(x), f_Q(x)] dx. \quad (1)$$

Definition 2 (Total Variation Distance). *The total variation distance $\delta : \mathbb{R}^n \times \mathbb{R}^n \rightarrow [0, 1]$ of the two distributions is defined as*

$$\delta(P, Q) = \frac{1}{2} \int_{\mathbb{R}^n} |f_P(x) - f_Q(x)| dx. \quad (2)$$

Definition 3 (Variation Distance on Subsets). *Given a subset A from \mathbb{R}^n , we define $\delta_A : \mathbb{R}^n \times \mathbb{R}^n \rightarrow [0, 1]$ to be the variation distance of the two distributions on A , which is*

$$\delta_A(P, Q) = \frac{1}{2} \int_A |f_P(x) - f_Q(x)| dx. \quad (3)$$

Remark 1. *One can prove that η and δ satisfy the following equation:*

$$\eta(P, Q) = 1 - \delta(P, Q) = 1 - \delta_A(P, Q) - \delta_{\mathbb{R}^n \setminus A}(P, Q). \quad (4)$$

The quantity δ_A defined in (3) will play an important role in deriving our upper bound for η .

B. The Upper Bound for the Overlap Index

We now proceed with deriving our proposed upper bound.

Theorem 1. *Without loss of generality, assume D^+ and D^- are two probability distributions on a bounded domain $B \subset \mathbb{R}^n$ with defined norm $\|\cdot\|$ (i.e., $\sup_{x \in B} \|x\| < +\infty$), then for any subset $A \subset B$ with its complementary set $A^c = B \setminus A$, we have*

$$\eta(D^+, D^-) \leq 1 - \frac{1}{2r_{A^c}} \|\mu_{D^+} - \mu_{D^-}\| - \frac{r_{A^c} - r_A}{r_{A^c}} \delta_A \quad (5)$$

where $r_A = \sup_{x \in A} \|x\|$ and $r_{A^c} = \sup_{x \in A^c} \|x\|$, μ_{D^+} and μ_{D^-} are the means of D^+ and D^- , and δ_A is the variation distance on set A defined in **Definition 3**. Moreover, let $r_B = \sup_{x \in B} \|x\|$, then we have

$$\eta(D^+, D^-) \leq 1 - \frac{1}{2r_B} \|\mu_{D^+} - \mu_{D^-}\| - \frac{r_B - r_A}{r_B} \delta_A. \quad (6)$$

Since (6) holds for any A , a tighter bound can be written as

$$\eta(D^+, D^-) \leq 1 - \frac{1}{2r_B} \|\mu_{D^+} - \mu_{D^-}\| - \max_A \frac{r_B - r_A}{r_B} \delta_A. \quad (7)$$

Proof. See Appendix A. \square

Remark 2. *The only assumption in this theorem is that the probability distribution domain is bounded. However, almost all real-world applications satisfy the boundedness assumption since the data is bounded. Therefore, r_B can always be found (or at least a reasonable approximation can be found). Additionally, we can constrain A to be a bounded ball so that r_A is also known. Although the proof of this theorem involves probability density functions, the computation does not require knowing the probability density functions but only finite samples because we can use the law of large numbers to estimate $\|\mu_{D^+} - \mu_{D^-}\|$ and δ_A , which will be shown next.*

C. Approximating the Bound with Finite Samples

Let $g : B \rightarrow \{0, 1\}$ be a condition function² and define $A = \{x \mid g(x) = 1, x \in B\}$. According to the definition of δ_A and triangular inequality, it is trivial to prove that

$$\delta_A(D^+, D^-) \geq \frac{1}{2} |\mathbb{E}_{D^+}[g] - \mathbb{E}_{D^-}[g]|. \quad (8)$$

Calculating $\mathbb{E}_{D^+}[g]$ and $\mathbb{E}_{D^-}[g]$ is easy: one just needs to draw samples from D^+ and D^- , and then average their g values. Applying (8) into **Theorem 1** gives the following corollary:

Corollary 1. *Given D^+ , D^- , B , and $\|\cdot\|$ used in **Theorem 1**, let $A(g) = \{x \mid g(x) = 1, x \in B\}$ with any condition function $g : B \rightarrow \{0, 1\}$. Then, an upper bound for $\eta(D^+, D^-)$ that can be obtained by our approximation is*

$$\eta(D^+, D^-) \leq 1 - \frac{1}{2r_B} \|\mu_{D^+} - \mu_{D^-}\| - \quad (9)$$

$$\max_g \frac{r_B - r_{A(g)}}{2r_B} |\mathbb{E}_{D^+}[g] - \mathbb{E}_{D^-}[g]|. \quad (10)$$

¹In this paper, we use the L_2 norm. However, the choice of the norm is not unique and the analysis can be carried out using other norms as well.

²The condition function is an indicator function $\mathbb{1}\{\text{condition}\}$ that outputs 1 when the input satisfies the given condition and 0 otherwise.

Given several condition functions $\{g_j\}_{j=1}^k$ and finite sample sets (i.e., $\{x_i^+\}_{i=1}^n \sim D^+$ and $\{x_i^-\}_{i=1}^m \sim D^-$), Alg. 1 shows how to compute the RHS of (10).

Algorithm 1 ComputeBound($\{x_i^+\}_{i=1}^n, \{x_i^-\}_{i=1}^m, \{g_j\}_{j=1}^k$)

```

B ← {x1+, x2+, ..., xn+, x1-, x2-, ..., xm-} and rB ←
maxx ∈ B ||x||
Δμ ← || $\frac{1}{n} \sum_{i=1}^n x_i^+ - \frac{1}{m} \sum_{i=1}^m x_i^-$ ||
for j = 1 → k do
  A = {x | gj(x) = 1, x ∈ B} and rA ← maxx ∈ A ||x||
  sj ← (1 -  $\frac{r_A}{r_B}$ ) | $\frac{1}{n} \sum_{i=1}^n g_j(x_i^+) - \frac{1}{m} \sum_{i=1}^m g_j(x_i^-)$ |
end for
Return: 1 -  $\frac{1}{2r_B} \Delta_\mu - \frac{1}{2} \max_j s_j$ 

```

Remark 3. *The choice of condition functions is not unique. In this work, we use the indicator function $g(x) = \mathbb{1}\{\|x\| \leq r\}$, which outputs 1 if $\|x\| \leq r$ and 0 otherwise. By setting different values for r , we generate a family of condition functions. The motivation for choosing such indicator function form is that it is the most simple way to separate a space nonlinearly and it saves computations by directly applying r into **Corollary 1**. However, other indicator functions, such as RBF kernel-based indicator functions, are worth exploring and will be considered in our future works.*

III. APPLICATION OF OUR BOUND TO ONE-CLASS CLASSIFICATION

A. Problem Formulation for One-Class Classification

Given \mathbb{R}^d space and n samples $\{x_i\}_{i=1}^n$ that lie in an unknown probability distribution, we would like to build a test $\Psi : \mathbb{R}^d \rightarrow \{\pm 1\}$ so that for any new input x , $\Psi(x)$ outputs 1 when x is from the same unknown probability distribution, and outputs -1, otherwise. Some applications of Ψ are novelty detection, out-of-distribution detection, and backdoor detection (e.g., Fig. 1(b, c)).

B. A Novel Confidence Score Function

Given some in-class samples $\{x_i\}_{i=1}^n$, one can pick several condition functions $\{g_j\}_{j=1}^k$, where $g_j(x) = \mathbb{1}\{\|x\| \leq r_j\}$ for different r_j , so that $f(x) = \text{ComputeBound}(\{x\}, \{x_i\}_{i=1}^n, \{g_j\}_{j=1}^k)$ defined in Alg. 1 is a score function that measures the likelihood of any input, x , being an in-class sample. Alg. 2 shows the overall one-class classification algorithm.

Algorithm 2 The Novel One-Class Classifier for the Input x

```

Given in-class samples  $\{x_i\}_{i=1}^n$ , select several condition
functions  $\{g_j\}_{j=1}^k$ , set a threshold  $T_0$ 
if ComputeBound( $\{x\}, \{x_i\}_{i=1}^n, \{g_j\}_{j=1}^k$ ) ≥  $T_0$  then
  x is an in-class sample
else
  x is an out-class sample
end if

```

Remark 4. The score function f measures the maximum similarity between the new input x and the available in-class samples $\{x_i\}_{i=1}^n$. Different T_0 lead to different detection accuracy. However, we will show that the proposed one-class classifier has an overall high accuracy under different T_0 .

C. Computation and Space Complexities

Our algorithm can pre-compute and store $\frac{1}{n} \sum_{i=1}^n x_i$ and $\frac{1}{n} \sum_{i=1}^n g_j(x_i)$ with $j = 1, 2, \dots, k$. Therefore, the total space complexity is $\mathcal{O}(k+1)$. Assume that the total number of new online inputs is l ; then, for every new input x , our algorithm needs to calculate $\|x\|$ once and s_j for k times. Therefore, the total computation complexity is $\mathcal{O}(l(k+1))$. Empirically, we restricted k to be a small number (e.g., 10) so that even devices without strong computation power can run our algorithm efficiently. Therefore, our classifier is computation-efficient and memory-efficient.

D. Evaluation

Overall Setup: We used $r_j = \frac{j}{k} r_B$ with $k = 50$ and r_B defined in **Theorem 1** unless specified. All the baseline algorithms with optimal hyperparameters, related datasets, and models were acquired from the corresponding authors' websites. The only exception is backdoor detection, in which we created our own models. However, we have carefully fine-tuned the baseline methods' hyperparameters to ensure their best performance over other hyperparameter choices.

1) *Novelty Detection:* We evaluated our classifier on 100 small UCI datasets [44], [45] and recorded the area under the receiver operating characteristic curve (AUROC). Fig. 2 shows the mean and standard deviation of AUROC for ours and other classifiers. Detailed numerical results are in Table IV in Appendix A. The implementation code is provided in the supplementary material.

Our classifier outperforms all the baseline methods by showing the highest average and lowest standard deviation of AUROC. Besides the results, our classifier is distribution-free, computation-efficient, and memory-efficient, whereas some other classifiers do not. Our method is also easy to explain and understand: the score measures the maximum similarity between the new input and the available in-class samples. Therefore, we conclude that our classifier is valid for novelty detection.

2) *Out-of-Distribution Detection:* We used CIFAR-10 and CIFAR-100 testing datasets [46] as the in-distribution datasets. The compared methods contain MSP [26], Mahalanobis [5], Energy score [27], and GEM [25]. We used WideResNet [47] to extract features from the raw data. The WideResNet models (well-trained on CIFAR-10 and CIFAR-100 training datasets) and corresponding feature extractors were acquired from [25]. All the methods were evaluated in the same feature spaces with their optimal hyperparameters for fair comparisons. To fit the score function's parameters for all the methods, we formed a small dataset by randomly selecting 10 samples from each class. The out-of-distribution datasets include Textures [48], SVHN [49], LSUN-Crop [50], LSUN-Resize [50], and iSUN [51]. We used three metrics: the detection accuracy for

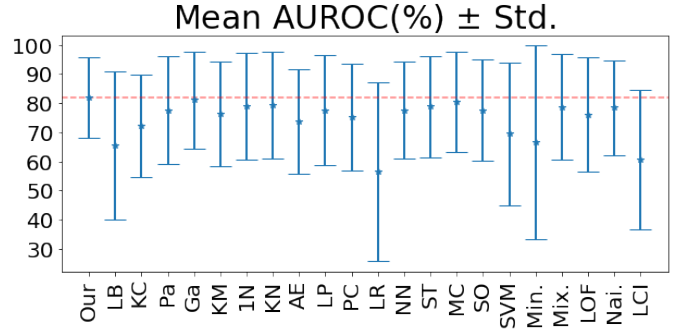


Fig. 2. Evaluation on 100 small UCI datasets for novelty detection. Details are in Table IV.

out-of-distribution samples when the detection accuracy for in-distribution samples is 95% (TPR95), AUROC, and area under precision and recall (AUPR).

Table I shows the average results for CIFAR-10 and CIFAR-100. The details for each individual out-of-distribution dataset can be found in Tables V and VI in Appendix A. Our method outperforms the other methods by using the least memory and showing the highest TPR95 and AUROC on average. The AUPR of our approach is in the same range as other baseline methods and the execution time of our approach for each sample is around 3 milliseconds (ms). We further evaluated our approach by using different numbers of indicator functions k and plotted the results in Fig. 3. From the figure, the performance of our approach increases with more indicator functions being used and eventually converges to a limit. This limit is determined by the out-of-distribution dataset, the tightness of our bound in **Corollary 1**, and the form of utilized indicator functions.

We also evaluated our approach with balanced datasets because the above out-of-distribution datasets are much different in size from the in-distribution datasets. On balanced datasets, our approach shows higher AUPR than the baseline methods as shown in Table II with details in Table VII in Appendix A. We also empirically observed that the compared baseline methods reported errors when data dimensions are dependent because the compared baseline methods need to calculate the inverse of the estimated covariance matrices that will not be full rank if data dimensions are dependent. We have reported this observation in Table VII in the appendix. In contrast, our approach works since it does not require finding the inverse of any matrices. Further, Table I and Table II together show that the baseline methods perform well only for out-of-distribution detection, whereas our approach performs well for both out-of-distribution detection and backdoor detection (details are explained in next subsection). In summary, our classifier is a valid out-of-distribution detector.

3) *Backdoor Detection:* The utilized datasets are MNIST [52], CIFAR-10 [46], GTSRB [53], YouTube Face [54], and sub-ImageNet [55]. The adopted backdoor attacks include naive triggers, all-label attacks [28], moving triggers [40], Wanet [32], combination attacks, large-sized triggers, filter triggers, and invisible sample-specific triggers [33], as listed

TABLE I
AVERAGE PERFORMANCE ON VARIOUS OUT-OF-DISTRIBUTION DATASETS. DETAILS ARE IN TABLES V AND VI.

In-Distributions	Method	TPR95	AUROC	AUPR	Time/Sample	Memory
CIFAR-10	Ours	81.39%	96.08%	96.17%	3.0ms	1048.22MiB
	MSP	50.63%	91.46%	98.07%	0.02ms	1825.21MiB
	Mahala.	46.83%	90.46%	97.92%	30.61ms	1983.17MiB
	Energy	68.31%	92.32%	97.96%	0.22ms	1830.01MiB
	GEM	50.81%	90.45%	97.91%	25.62ms	1983.51MiB
CIFAR-100	Ours	72.93%	93.53%	93.69%	3.0ms	1134.32MiB
	MSP	19.87%	75.97%	94.09%	0.02ms	1825.98MiB
	Mahala.	48.35%	84.90%	96.37%	56.24ms	1983.81MiB
	Energy	27.91%	80.44%	95.15%	0.21ms	1838.23MiB
	GEM	48.36%	84.94%	96.38%	56.27ms	1984.77MiB

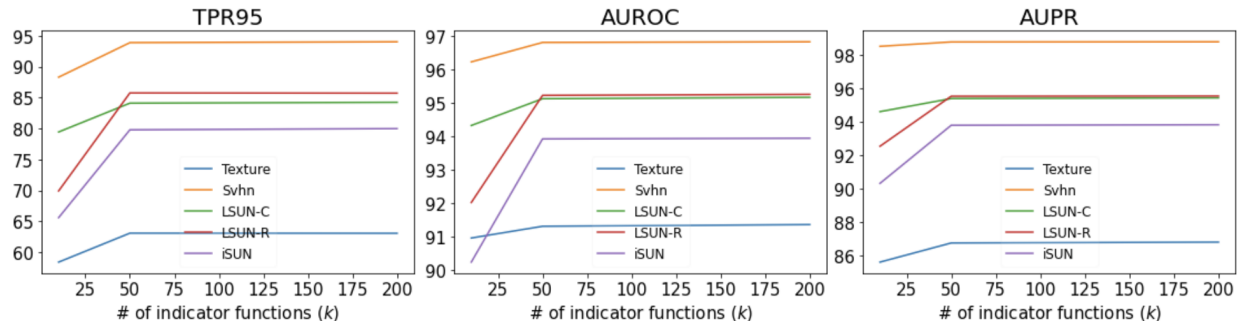


Fig. 3. Performance of our approach with different k when CIFAR-10 is the in-distribution data.

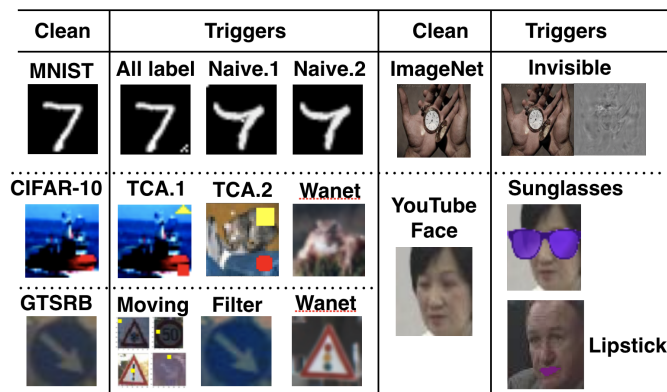


Fig. 4. Pictures under "Triggers" are poisoned samples regarding different backdoored attacks. Pictures under "Clean" are clean samples for each dataset.

in Fig. 4. The neural network architecture includes Network in Network [56], Resnet [57], and other networks from [36], [28]. For each backdoor attack, we assume that a small clean validation dataset is available (i.e., 10 samples from each class) at the beginning. Therefore, the poisoned samples (i.e., samples attached with triggers) can be considered out-class samples, whereas the clean samples can be considered in-class samples. We used the backdoored network to extract data features. Then, we evaluated our one-class classifier and compared it with the previous baseline methods and STRIP [38] in the feature space. The metrics used are the same: TPR95 (i.e., the detection accuracy for poisoned samples when the detection accuracy for clean samples is 95%), AUROC, and AUPR. Table II shows the average performance. Details

TABLE II
AVERAGE PERFORMANCE FOR BACKDOOR DETECTION OVER VARIOUS BACKDOOR TRIGGERS AND DATASETS.

Metrics (%)	Ours	STRIP	Mahalanobis	GEM	MSP
TPR95	89.40	39.60	56.97	91.57	39.24
AUROC	96.68	70.30	75.94	58.08	54.92
AUPR	95.42	68.76	76.37	75.88	60.52

on each individual trigger can be found in Table VII in Appendix A

From the table, our classifier outperforms other baseline methods on average by showing the highest AUROC and AUPR. Additionally, our approach also has a very high TPR95. For each individual trigger, the TPR95 of our method is over 96% for most cases, the AUROC of our method is over 97% for most cases, and the AUPR of our method is over 95% for most cases. It is also seen that our classifier is robust against the latest or advanced backdoor attacks, such as Wanet, invisible trigger, all label attack, and filter attack, whereas the baseline methods show low performance on those attacks. Therefore, we conclude that our classifier is valid for backdoor detection.

4) *Anomaly Detection with Iterative Scores*: For an input x , denote the confidence score calculated using the condition functions $g_j(x) = \mathbb{1}\{|x| \leq r_j\}$ as $s(x)$, then its iterative confidence score, $s'(x)$, is calculated by Alg. 1 but with the new condition functions $g'_j(x) = \mathbb{1}\{s(x) \leq \frac{j}{k}\}$. To evaluate the efficacy of this iterative approach, we consider the comparison with deep network-based classifiers, including DCAE [58], AnoGAN [59], Deep SVDD [23], and OCGAN [24], for anomaly detection on the CIFAR-10 dataset in the raw image space. The anomaly detection setting considers one

class as normal and the remaining classes as anomalous. The baseline methods need to first train deep networks on available normal-class samples and then use the trained models to detect anomalies, whereas our approach does not require this training process. Additionally, we empirically observed that the baseline methods require around 5000 available normal-class training samples to be effective, whereas our approach needs only 100 available normal samples to be effective. For a fair comparison, we allow the baseline methods to use 5000 available normal-class samples to train their deep networks to achieve their best performance.

Table III shows the results. Our approach shows the highest AUROC on average. Additionally, our approach shows either the best or the second-best performance for 9 individual cases. Moreover, if the baseline methods are trained with only 100 available normal samples, then their performance will become lower. For example, Deep SVDD shows only 61.1% AUROC on average. Therefore, our approach is valid and sample-efficient in the raw image space and outperforms the deep network-based anomaly detection methods.

IV. APPLICATION OF OUR BOUND TO DOMAIN SHIFT ANALYSIS

Our bound is also useful in domain shift analysis.

Theorem 2. Assume that D and D^* are two different data distributions (i.e., $\eta(D, D^*) < 1$) and denote the overall accuracy of the model on D^* as Acc . If a model is trained on D with p accuracy on D and q accuracy on $D^* \setminus D$, then we have

$$Acc \leq (p - q) \left(1 - \frac{1}{2r_B} \|\mu_D - \mu_{D^*}\| - \right) \quad (11)$$

$$\max_g \frac{r_B - r_{A(g)}}{2r_B} |\mathbb{E}_D[g] - \mathbb{E}_{D^*}[g]| + q. \quad (12)$$

Proof. See Appendix A. \square

Remark 5. As one case of the domain shift, a backdoor attack scenario (Fig. 1(b)) considers that the model has a zero accuracy on poisoned data distribution (i.e., $q = 0$) as the attack success rate is almost 100%. Define the clean data distribution as D , poisoned data distribution as D^p , and a testing data distribution D^* composed by D and D^p , i.e., $D^* = \sigma D + (1 - \sigma)D^p$, where $\sigma \in [0, 1]$ is the purity ratio (i.e., the ratio of clean samples to the entire testing samples). Then (12) becomes

$$Acc \leq p \left(1 - \frac{1 - \sigma}{2r_B} \|\mu_D - \mu_{D^p}\| - \right) \quad (13)$$

$$(1 - \sigma) \max_g \frac{r_B - r_{A(g)}}{2r_B} |\mathbb{E}_D[g] - \mathbb{E}_{D^p}[g]|. \quad (14)$$

Experimental Illustration of Theorem 2: The backdoor attack scenario is used to illustrate Theorem 2 using MNIST, GTSRB, YouTube Face, and sub-ImageNet datasets and their domain-shifted versions shown in “All label” for MNIST, “Filter” for GTSRB, “Sunglasses” for YouTube Face, and “Invisible” for sub-ImageNet in Fig. 4. We composed the testing datasets D^* with $\sigma = 0, 0.1, \dots, 0.9, 1$ and calculated the RHS of (14) using L_1 , L_2 , and L_∞ norms in the raw image

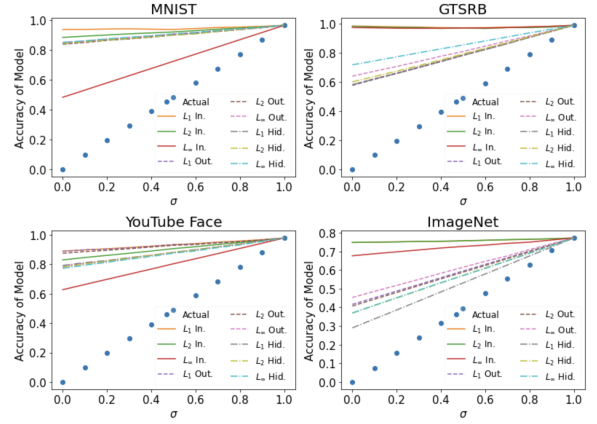


Fig. 5. The actual model accuracy (dot) vs. (12) (solid) calculated with L_1 , L_2 , and L_∞ norms in input, output, and hidden spaces. x : the ratio of clean samples to the entire testing samples.

space, model output space, and hidden layer space. Fig. 5 shows the actual model accuracy and corresponding upper bounds with different σ s. The actual model accuracy is below all the calculated upper limits, which validates **Theorem 2**.

Additionally, the difference between actual model accuracy and the calculated upper bound accuracy can reflect the extent of the domain shift in the test dataset. From Fig. 5, a large difference reflects a large domain shift. When the domain shift vanishes, the actual model accuracy and the calculated upper bound accuracy coincide. Compared to other methods, our approach is time-efficient.

Theorem 2 can also help infer useful data information to most likely find and remove domain-shifted samples to eliminate the domain shift. Specifically, from Fig. 5, the calculated upper bound accuracy varies with norms and feature spaces. The inference is that a low calculated upper bound accuracy implies a high likelihood of distinguishing original and domain-shifted data distributions in that particular utilized feature space. For example, in Fig. 5 MNIST and YouTube, the input space with L_∞ norm shows the lowest calculated upper bound accuracy. Therefore, the inference is that the original and domain-shifted data distributions are likely to be distinguished in the raw image space. Indeed, even vision inspection can easily distinguish original and domain-shifted samples for the MNIST and YouTube cases given their domain-shifted samples under “All label” and “Sunglasses” in Fig. 4. As for GTSRB and ImageNet, the input space has the highest upper limit lines. Therefore, the original and domain-shifted data distributions are less likely to be distinguished in the raw image space. Since their domain-shifted samples are “Filter” and “Invisible” in Fig. 4, the vision inspection barely discriminates between original and domain-shifted samples for GTSRB and sub-ImageNet. Moreover, the hidden layer space gives the lowest estimated upper bound accuracy for GTSRB and ImageNet. Therefore, original and domain-shifted samples are more likely to be visually distinguished in the hidden layer space as shown in Fig. 6.

TABLE III
AUROC (%) ON CIFAR-10 WITH DIFFERENT NORMAL CLASSES. **Boldface** SHOWS THE BEST PERFORMING ALGORITHM, WHEREAS UNDERLINE SHOWS THE SECOND BEST ALGORITHM.

Methods	Air.	Aut.	Bird	Cat	Deer	Dog	Frog	Hor.	Ship	Tru.	Ave.
Ours	<u>75.0</u>	67.9	<u>56.9</u>	<u>60.4</u>	<u>68.6</u>	<u>63.1</u>	69.9	61.0	<u>77.9</u>	76.0	67.7
OCGAN	75.7	53.1	64.0	62.0	72.3	62.0	72.3	57.5	82.0	55.4	<u>65.6</u>
Deep SVDD	61.7	<u>65.9</u>	50.8	59.1	60.9	65.7	67.7	67.3	75.9	<u>73.1</u>	64.8
AnoGAN	67.1	<u>54.7</u>	52.9	54.5	65.1	60.3	58.5	<u>62.5</u>	75.8	66.5	61.8
DCAE	59.1	57.4	48.9	58.4	54.0	62.2	51.2	58.6	76.8	67.3	59.4

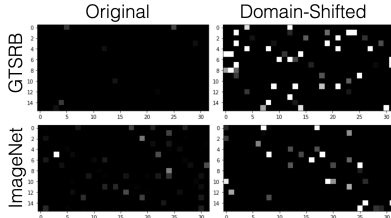


Fig. 6. Original and domain-shifted sample in the hidden layer space.

V. CONCLUSION

This paper proposes an easy-to-compute distribution-free upper bound for the distribution overlap index. The computation of the bound is time-efficient and memory-efficient and only requires finite samples. Two applications of the bound are explored. The first application is for one-class classification. Specifically, this paper introduces a novel distribution-free one-class classifier with the bound being its confidence score function. The classifier is sample-efficient, computation-efficient, and memory-efficient. The proposed classifier is evaluated on novelty detection, out-of-distribution detection, backdoor detection, and anomaly detection on various datasets and outperforms many state-of-the-art methods. The second application is for domain shift analysis with a proposed theorem to detect the domain shift existence and infer useful data information. The obtained results show significant promise toward broadening the application of overlap-based metrics.

REFERENCES

- [1] H. Fu, P. Krishnamurthy, and F. Khorrani, "Functional replicas of proprietary three-axis attitude sensors via lstm neural networks," in *2020 IEEE Conference on Control Technology and Applications*. IEEE, 2020, pp. 70–75.
- [2] A. Papanicolaou, H. Fu, P. Krishnamurthy, B. Healy, and F. Khorrani, "An optimal control strategy for execution of large stock orders using long short-term memory networks," *Journal of Computational Finance*, vol. 26, no. 4, 2023.
- [3] A. Papanicolaou, H. Fu, P. Krishnamurthy, and F. Khorrani, "A deep neural network algorithm for linear-quadratic portfolio optimization with mgarch and small transaction costs," *IEEE Access*, vol. 11, pp. 16 774–16 792, 2023.
- [4] A. Sarmadi, H. Fu, P. Krishnamurthy, S. Garg, and F. Khorrani, "Privacy-preserving collaborative learning through feature extraction," *IEEE Transactions on Dependable and Secure Computing*, vol. 21, no. 1, pp. 486–498, 2023.
- [5] K. Lee, K. Lee, H. Lee, and J. Shin, "A simple unified framework for detecting out-of-distribution samples and adversarial attacks," in *Proceedings of Advances in Neural Information Processing Systems*, vol. 31, Montreal, Canada, Dec. 2018.
- [6] B. Schölkopf, J. C. Platt, J. Shawe-Taylor, A. J. Smola, and R. C. Williamson, "Estimating the support of a high-dimensional distribution," *Neural Computation*, vol. 13, no. 7, pp. 1443–1471, 2001.
- [7] C. Gini and G. Livada, "Nuovi contributi alla teoria della transvariazione," *Roma: Atti della VI Riunione della Società Italiana di Statistica*, 1943.
- [8] M. S. Weitzman, *Measures of overlap of income distributions of white and Negro families in the United States*. US Bureau of the Census, 1970, vol. 3.
- [9] S. Kullback and R. A. Leibler, "On information and sufficiency," *The Annals of Mathematical Statistics*, vol. 22, no. 1, pp. 79–86, 1951.
- [10] A. Bhattacharyya, "On a measure of divergence between two statistical populations defined by their probability distributions," *Bulletin of the Calcutta Mathematical Society*, vol. 35, pp. 99–109, 1943.
- [11] E. Hellinger, "Neue begründung der theorie quadratischer formen von unendlichvielen veränderlichen," *Journal für die reine und angewandte Mathematik*, vol. 1909, no. 136, pp. 210–271, 1909.
- [12] J. Cohen, *Statistical power analysis for the behavioral sciences*. Routledge, 2013.
- [13] K. O. McGraw and S. P. Wong, "A common language effect size statistic," *Psychological Bulletin*, vol. 111, no. 2, p. 361, 1992.
- [14] C. J. Huberty and L. L. Lowman, "Group overlap as a basis for effect size," *Educational and Psychological Measurement*, vol. 60, no. 4, pp. 543–563, 2000.
- [15] M. Pastore and A. Calcagni, "Measuring distribution similarities between samples: A distribution-free overlapping index," *Frontiers in Psychology*, vol. 10, p. 1089, 2019.
- [16] M. M. Moya and D. R. Hush, "Network constraints and multi-objective optimization for one-class classification," *Neural Networks*, vol. 9, no. 3, pp. 463–474, 1996.
- [17] H. Fu, P. Krishnamurthy, and F. Khorrani, "Combining switching mechanism with re-initialization and anomaly detection for resiliency of cyber-physical systems," *Automatica*, vol. 172, p. 111994, 2025.
- [18] H. Fu, N. Patel, P. Krishnamurthy, and F. Khorrani, "Clipscope: Enhancing zero-shot ood detection with bayesian scoring," *arXiv preprint arXiv:2405.14737*, 2024.
- [19] J. Yang, K. Zhou, Y. Li, and Z. Liu, "Generalized out-of-distribution detection: A survey," *arXiv preprint arXiv:2110.11334*, 2021.
- [20] S. S. Khan and M. G. Madden, "One-class classification: taxonomy of study and review of techniques," *The Knowledge Engineering Review*, vol. 29, no. 3, pp. 345–374, 2014.
- [21] F. D. Comité, F. Denis, R. Gilleron, and F. Letouzey, "Positive and unlabeled examples help learning," in *Proceedings of International Conference on Algorithmic Learning Theory*, Tokyo, Japan, Dec. 1999, pp. 219–230.
- [22] D. M. J. Tax, "One-class classification: Concept learning in the absence of counter-examples," Ph.D. dissertation, Technische Universiteit Delft, 2002.
- [23] L. Ruff, R. Vandermeulen, N. Goernitz, L. Deecke, S. A. Siddiqui, A. Binder, E. Müller, and M. Kloft, "Deep one-class classification," in *Proceedings of International Conference on Machine Learning*, Stockholm, Sweden, July 2018, pp. 4393–4402.
- [24] P. Perera, R. Nallapati, and B. Xiang, "Ocgan: One-class novelty detection using gans with constrained latent representations," in *Proceedings of the IEEE/CVF Conference on Computer Vision and Pattern Recognition*, Long Beach, CA, June 2019, pp. 2898–2906.
- [25] P. Morteza and Y. Li, "Provable guarantees for understanding out-of-distribution detection," in *Proceedings of the AAAI Conference on Artificial Intelligence*, vol. 8, Virtual, Feb. 2022.
- [26] D. Hendrycks and K. Gimpel, "A baseline for detecting misclassified and out-of-distribution examples in neural networks," in *Proceedings of International Conference on Learning Representations*, Toulon, France, Apr. 2017.
- [27] W. Liu, X. Wang, J. Owens, and Y. Li, "Energy-based out-of-distribution detection," in *Proceedings of Advances in Neural Information Processing Systems*, vol. 33, Virtual, Dec. 2020, pp. 21 464–21 475.

- [28] T. Gu, K. Liu, B. Dolan-Gavitt, and S. Garg, “Badnets: Evaluating backdooring attacks on deep neural networks,” *IEEE Access*, vol. 7, pp. 47 230–47 244, 2019.
- [29] Y. Liu, S. Ma, Y. Aafer, W.-C. Lee, J. Zhai, W. Wang, and X. Zhang, “Trojaning attack on neural networks,” in *Proceedings of the Network and Distributed Systems Security Symposium*, San Diego, CA, Feb. 2018.
- [30] B. Biggio, B. Nelson, and P. Laskov, “Poisoning attacks against support vector machines,” in *Proceedings of the International Conference on International Conference on Machine Learning*, Edinburgh, Scotland, June 2012, pp. 1467–1474.
- [31] I. Goodfellow, J. Pouget-Abadie, M. Mirza, B. Xu, D. Warde-Farley, S. Ozair, A. Courville, and Y. Bengio, “Generative adversarial nets,” in *Proceedings of Advances in Neural Information Processing Systems*, vol. 27, Montreal, Canada, Dec. 2014.
- [32] T. A. Nguyen and A. T. Tran, “Wanet - imperceptible warping-based backdoor attack,” in *Proceedings of the International Conference on Learning Representations*, Virtual, May 2021.
- [33] Y. Li, Y. Li, B. Wu, L. Li, R. He, and S. Lyu, “Invisible backdoor attack with sample-specific triggers,” in *Proceedings of the IEEE/CVF International Conference on Computer Vision*, Virtual, June 2021, pp. 16 463–16 472.
- [34] Y. Zeng, W. Park, Z. M. Mao, and R. Jia, “Rethinking the backdoor attacks’ triggers: A frequency perspective,” in *Proceedings of the IEEE/CVF International Conference on Computer Vision*, 2021, pp. 16 473–16 481.
- [35] Y. Liu, X. Ma, J. Bailey, and F. Lu, “Reflection backdoor: A natural backdoor attack on deep neural networks,” in *Proceedings of the European Conference on Computer Vision*, Virtual, Aug. 2020, pp. 182–199.
- [36] B. Wang, Y. Yao, S. Shan, H. Li, B. Viswanath, H. Zheng, and B. Y. Zhao, “Neural cleanse: Identifying and mitigating backdoor attacks in neural networks,” in *Proceedings of IEEE Symposium on Security and Privacy*, San Francisco, CA, May 2019, pp. 707–723.
- [37] K. Liu, B. Dolan-Gavitt, and S. Garg, “Fine-pruning: Defending against backdooring attacks on deep neural networks,” in *Proceedings of International Symposium on Research in Attacks, Intrusions, and Defenses*, Crete, Greece, Sep. 2018, pp. 273–294.
- [38] Y. Gao, C. Xu, D. Wang, S. Chen, D. C. Ranasinghe, and S. Nepal, “Strip: A defence against trojan attacks on deep neural networks,” in *Proceedings of the Annual Computer Security Applications Conference*, Austin, TX, Dec. 2019, pp. 113–125.
- [39] A. K. Veldanda, K. Liu, B. Tan, P. Krishnamurthy, F. Khorrami, R. Karri, B. Dolan-Gavitt, and S. Garg, “Nnoculation: Catching badnets in the wild,” in *Proceedings of the ACM Workshop on Artificial Intelligence and Security*, Virtual, Nov. 2021, pp. 49–60.
- [40] H. Fu, A. K. Veldanda, P. Krishnamurthy, S. Garg, and F. Khorrami, “A feature-based on-line detector to remove adversarial-backdoors by iterative demarcation,” *IEEE Access*, vol. 10, pp. 5545 – 5558, 2022.
- [41] H. Fu, P. Krishnamurthy, S. Garg, and F. Khorrami, “Differential analysis of triggers and benign features for black-box dnn backdoor detection,” *IEEE Transactions on Information Forensics and Security*, vol. 18, pp. 4668–4680, 2023.
- [42] H. Fu, “Enhancing the safety of machine learning systems and cyber-physical systems against cyber attacks,” Ph.D. dissertation, New York University Tandon School of Engineering, 2024.
- [43] H. Fu, A. Sarmadi, P. Krishnamurthy, S. Garg, and F. Khorrami, “Mitigating backdoor attacks on deep neural networks,” in *Embedded Machine Learning for Cyber-Physical, IoT, and Edge Computing: Use Cases and Emerging Challenges*. Springer, 2023, pp. 395–431.
- [44] “One-class classifier results,” <http://homepage.tudelft.nl/n9d04/occl/index.html>, accessed: 2022-08-30.
- [45] D. Dua and C. Graff, “UCI machine learning repository,” 2017. [Online]. Available: <http://archive.ics.uci.edu/ml>
- [46] A. Krizhevsky, G. Hinton *et al.*, “Learning multiple layers of features from tiny images,” 2009.
- [47] S. Zagoruyko and N. Komodakis, “Wide residual networks,” *arXiv preprint arXiv:1605.07146*, 2016.
- [48] M. Cimpoi, S. Maji, I. Kokkinos, S. Mohamed, and A. Vedaldi, “Describing textures in the wild,” in *Proceedings of the IEEE Conference on Computer Vision and Pattern Recognition*, Columbus, OH, June 2014, pp. 3606–3613.
- [49] Y. Netzer, T. Wang, A. Coates, A. Bissacco, B. Wu, and A. Y. Ng, “Reading digits in natural images with unsupervised feature learning,” in *Proceedings of NIPS Workshop on Deep Learning and Unsupervised Feature Learning*, Granada, Spain, Dec. 2011.
- [50] F. Yu, A. Seff, Y. Zhang, S. Song, T. Funkhouser, and J. Xiao, “Lsun: Construction of a large-scale image dataset using deep learning with humans in the loop,” *arXiv preprint arXiv:1506.03365*, 2015.
- [51] P. Xu, K. A. Ehinger, Y. Zhang, A. Finkelstein, S. R. Kulkarni, and J. Xiao, “Turkergaze: Crowdsourcing saliency with webcam based eye tracking,” *arXiv preprint arXiv:1504.06755*, 2015.
- [52] Y. LeCun, C. Cortes, and C. Burges, “Mnist handwritten digit database,” *ATT Labs [Online]*. Available: <http://yann.lecun.com/exdb/mnist>, vol. 2, 2010.
- [53] J. Stalkamp, M. Schlipf, J. Salmen, and C. Igel, “The german traffic sign recognition benchmark: A multi-class classification competition,” in *Proceedings of the International Joint Conference on Neural Networks*, San Jose, CA, July 2011, pp. 1453–1460.
- [54] L. Wolf, T. Hassner, and I. Maoz, “Face recognition in unconstrained videos with matched background similarity,” in *Proceedings of the IEEE Conference on Computer Vision and Pattern Recognition*, Colorado Springs, CO, June 2011, pp. 529–534.
- [55] J. Deng, W. Dong, R. Socher, L. Li, Kai Li, and Li Fei-Fei, “Imagenet: A large-scale hierarchical image database,” in *Proceedings of the IEEE Conference on Computer Vision and Pattern Recognition*, Miami, FL, 2009, pp. 248–255.
- [56] M. Lin, Q. Chen, and S. Yan, “Network in network,” in *Proceedings of the International Conference on Learning Representations*, Banff, Canada, Apr. 2014, pp. 1–10.
- [57] K. He, X. Zhang, S. Ren, and J. Sun, “Deep residual learning for image recognition,” in *Proceedings of the IEEE Conference on Computer Vision and Pattern Recognition*, Miami, FL, June 2016, pp. 770–778.
- [58] A. Makhzani and B. J. Frey, “Winner-take-all autoencoders,” in *Advances in Neural Information Processing Systems*, C. Cortes, N. Lawrence, D. Lee, M. Sugiyama, and R. Garnett, Eds., vol. 28, Montréal, Canada, Dec. 2015, p. 2791–2799.
- [59] T. Schlegl, P. Seeböck, S. M. Waldstein, U. Schmidt-Erfurth, and G. Langs, “Unsupervised anomaly detection with generative adversarial networks to guide marker discovery,” in *International Conference on Information Processing in Medical Imaging*. Springer, 2017, pp. 146–157.

APPENDIX

Proof. Let f_{D^+} and f_{D^-} be the probability density functions for D^+ and D^- . From (4), we have

$$\eta(D^+, D^-) = 1 - \delta_A(D^+, D^-) - \delta_{A^c}(D^+, D^-). \quad (15)$$

Using (15), triangular inequality, and boundedness, we obtain

$$\|\mu_{D^+} - \mu_{D^-}\| = \left\| \int_B x (f_{D^+}(x) - f_{D^-}(x)) dx \right\| \leq \int_B \|x(f_{D^+}(x) - f_{D^-}(x))\| dx \quad (16)$$

$$= \int_A \|x\| \cdot |f_{D^+}(x) - f_{D^-}(x)| dx + \int_{A^c} \|x\| \cdot |f_{D^+}(x) - f_{D^-}(x)| dx \quad (17)$$

$$\leq 2r_A \delta_A + 2r_{A^c} \delta_{A^c} = 2r_A \delta_A + 2r_{A^c} (1 - \delta_A - \eta(D^+, D^-)) \quad (18)$$

which implies (5). Replacing r_{A^c} with r_B in (18) implies (6). \square

Proof. Let f_D and f_{D^*} be their probability density functions, then

$$Acc = \int_{x \sim D^*} \left(p \frac{\min\{f_D(x), f_{D^*}(x)\}}{f_{D^*}(x)} + q \left(1 - \frac{\min\{f_D(x), f_{D^*}(x)\}}{f_{D^*}(x)} \right) \right) f_{D^*}(x) dx \quad (19)$$

$$= p\eta(D, D^*) + q(1 - \eta(D, D^*)) = (p - q)\eta(D, D^*) + q \quad (20)$$

$$\leq (p - q) \left(1 - \frac{1}{2r_B} \|\mu_D - \mu_{D^*}\| - \max_g \frac{r_B - r_{A(g)}}{2r_B} |\mathbb{E}_D[g] - \mathbb{E}_{D^*}[g]| \right) + q. \quad (21)$$

\square

The method in Table IV is in the same order as shown in Fig. 2. Table V is for CIFAR-10 case and Table VI is for

TABLE IV
MEANS AND STANDARD DEVIATIONS OF AUROC (%) FOR DIFFERENT METHODS ON 100 UCI DATASETS.

Ours	L1-Ball	K-Center	Parzen	Gaussian	K-Mean
81.9 ± 13.8	65.4 ± 25.4	72.2 ± 17.6	77.6 ± 18.6	81.1 ± 16.6	76.3 ± 17.9
1-Nearest	K-Nearest	Auto-Encoder	Linear	Principal	Lof
Neighbor	Neighbor	Network	Programming	Component	Range
78.8 ± 18.3	79.2 ± 18.3	73.7 ± 17.9	77.5 ± 18.9	75.1 ± 18.3	56.5 ± 30.8
Nearest	Minimum	Minimum	Self	Support	Minimax
Neighbor	Spanning	Covariance	Organizing	Vector	Probability
Distance	Tree	Determinant	Map	Machine	Machine
77.5 ± 16.6	78.8 ± 17.4	80.4 ± 17.1	77.6 ± 17.4	69.4 ± 24.6	66.4 ± 33.3
Mixture	Local Outlier	Naive	Local Correlation		
Gaussians	Factor	Parzen	Integral		
78.7 ± 18.1	76.1 ± 19.7	78.4 ± 16.2	60.7 ± 23.9		

CIFAR-100 case.

Table VII shows the details for backdoor detection.

TABLE V
RESULTS FOR CIFAR-10 IN-DISTRIBUTION CASE (HIGHER NUMBER IMPLIES HIGHER ACCURACY). **Boldface** SHOWS THE BEST PERFORMING ALGORITHM, WHEREAS UNDERLINE SHOWS THE SECOND BEST ALGORITHM.

Out-of-Distribution Datasets	Method	TPR95 (%)	AUROC (%)	AUPR (%)
Texture	Ours	64.20	92.80	92.33
	MSP	40.75	88.31	97.08
	Mahalanobis	62.38	94.46	98.75
	Energy Score	47.47	85.47	95.58
	GEM	72.61	94.59	98.79
SVHN	Ours	94.10	98.56	99.41
	MSP	52.41	92.11	98.32
	Mahalanobis	<u>79.34</u>	<u>95.72</u>	<u>99.04</u>
	Energy Score	64.20	91.05	97.66
	GEM	79	95.65	99.01
LSUN-Crop	Ours	<u>83.63</u>	<u>96.60</u>	96.61
	MSP	69.07	95.64	<u>99.13</u>
	Mahalanobis	30.06	86.15	97.05
	Energy Score	91.89	98.40	99.67
	GEM	30.20	86.09	97.03
LSUN-Resize	Ours	85.41	96.84	96.86
	MSP	47.45	91.30	98.11
	Mahalanobis	35.64	88.12	97.45
	Energy Score	71.75	<u>94.12</u>	98.64
	GEM	35.45	88.09	97.43
iSUN	Ours	79.62	95.64	95.68
	MSP	43.40	89.72	<u>97.72</u>
	Mahalanobis	26.77	87.87	97.33
	Energy Score	<u>66.27</u>	<u>92.56</u>	98.25
	GEM	36.80	87.85	93.33
Average Performance	Ours	81.39	96.08	96.17
	MSP	50.63	91.46	98.07
	Mahalanobis	46.83	90.46	97.92
	Energy Score	68.31	<u>92.32</u>	<u>97.96</u>
	GEM	<u>50.81</u>	90.45	97.91

TABLE VI
RESULTS FOR CIFAR-100 IN-DISTRIBUTION CASE (HIGHER NUMBER IMPLIES HIGHER ACCURACY). **Boldface** SHOWS THE BEST PERFORMING ALGORITHM, WHEREAS UNDERLINE SHOWS THE SECOND BEST ALGORITHM.

Out-of-Distribution Datasets	Method	TPR95 (%)	AUROC (%)	AUPR (%)
Texture	Ours	42.50	85.79	85.27
	MSP	16.71	73.58	93.02
	Mahalanobis	57.62	<u>90.14</u>	<u>97.62</u>
	Energy Score	20.38	76.46	93.68
	GEM	<u>57.40</u>	90.17	97.63
SVHN	Ours	93.75	98.36	99.36
	MSP	15.66	71.37	92.89
	Mahalanobis	51.35	89.25	97.52
	Energy Score	14.59	74.10	93.65
	GEM	51.51	89.40	<u>97.57</u>
LSUN-Crop	Ours	<u>57.76</u>	<u>89.95</u>	90.03
	MSP	33.44	83.71	<u>96.32</u>
	Mahalanobis	1.53	58.48	89.73
	Energy Score	64.01	93.41	98.59
	GEM	1.70	58.42	89.70
LSUN-Resize	Ours	88.49	97.56	97.55
	MSP	16.54	75.32	94.03
	Mahalanobis	<u>67.20</u>	93.97	98.70
	Energy Score	21.38	79.29	94.97
	GEM	67.09	<u>94.01</u>	98.70
iSUN	Ours	82.15	96.05	96.24
	MSP	17.02	75.87	94.20
	Mahalanobis	64.07	92.69	98.32
	Energy Score	19.20	78.98	94.90
	GEM	<u>64.10</u>	<u>92.73</u>	98.32
Average Performance	Ours	72.93	93.53	93.69
	MSP	19.87	75.97	94.09
	Mahalanobis	48.35	84.90	<u>96.37</u>
	Energy Score	27.91	80.44	95.15
	GEM	<u>48.36</u>	<u>84.94</u>	96.38

TABLE VII
COMPARISON RESULTS FOR BACKDOOR DETECTION (HIGHER NUMBER IMPLIES HIGHER ACCURACY).

Datasets	Trigger	Metrics (%)	Ours	STRIP	Mahalanobis	GEM	MSP
MNIST	All label	TPR95	83.05	2.58	50.83	100	100
		AUROC	96.13	44.69	90.78	50.43	50
		AUPR	94.20	35.47	86.71	70.94	70.83
MNIST	Naive.1	TPR95	100	98.85	99.86	100	5.11
		AUROC	97.50	97.32	97.49	53.95	51.64
		AUPR	96.17	95.95	96.38	74.74	50.41
MNIST	Naive.2	TPR95	96.53	67.46	35.16	100	14.69
		AUROC	97.28	93.67	78.63	53.51	58.14
		AUPR	95.75	89.85	78.65	74.62	64.16
CIFAR-10	TCA.1	TPR95	100	35.68	100	100	4.38
		AUROC	97.50	83.00	97.49	50	49.23
		AUPR	95.47	73.22	97.84	76.32	52.64
CIFAR-10	TCA.2	TPR95	100	27.86	100	100	0.02
		AUROC	97.50	68.79	97.49	50	29.90
		AUPR	97.63	72.41	95.86	67.86	18.05
CIFAR-10	Wanet	TPR95	37.87	0.07	20.35	22.90	100
		AUROC	92.74	34.97	50.61	57.81	50
		AUPR	89.95	37.42	57.30	68.48	74.87
GTSRB	Moving	TPR95	99.99	54	Fail: dependent data dimensions		
		AUROC	85.39	7.29			
		AUPR	96.96	89.07			
GTSRB	Filter	TPR95	85.39	7.29	Fail: dependent data dimensions		
		AUROC	96.54	38.92			
		AUPR	95.42	38.81			
GTSRB	Wanet	TPR95	100	1.24	0.51	100	100
		AUROC	97.50	36.31	54.46	50	50
		AUPR	97.62	39.53	48.92	75.23	75.23
YouTube Face	Sunglasses	TPR95	73.37	83.03	71.64	98.58	13.06
		AUROC	95.21	94.80	94.38	84.29	66.55
		AUPR	93.00	95.54	94.63	88.83	53.27
YouTube Face	Lipstick	TPR95	96.64	90.14	90.88	94.18	3.73
		AUROC	97.21	93.15	93.26	80.80	50.14
		AUPR	96.30	94.98	95.09	86.53	53.27
sub-ImageNet	Invisible	TPR95	100	7.01	0.5	100	51.40
		AUROC	97.49	66.26	4.78	50	93.61
		AUPR	96.53	62.83	12.27	75.26	92.46
Average Performance		TPR95	89.40	39.60	56.97	91.57	39.24
		AUROC	96.68	70.30	75.94	58.08	54.92
		AUPR	95.42	68.76	76.37	75.88	60.52